Sea Ice Concentrations from Nimbus-7 SMMR and DMSP SSM/I-SSMIS Passive Microwave Data, Version 2

USER GUIDE

How to Cite These Data

As a condition of using these data, you must include a citation:

DiGirolamo, N. E., C. L. Parkinson, D. J. Cavalieri, P. Gloersen, and H. J. Zwally. 2022, updated yearly. *Sea Ice Concentrations from Nimbus-7 SMMR and DMSP SSM/I-SSMIS Passive Microwave Data, Version 2*. [Indicate subset used]. Boulder, Colorado USA. NASA National Snow and Ice Data Center Distributed Active Archive Center. https://doi.org/10.5067/MPYG15WAA4WX. [Date Accessed].

FOR QUESTIONS ABOUT THESE DATA, CONTACT NSIDC@NSIDC.ORG

FOR CURRENT INFORMATION, VISIT https://nsidc.org/data/NSIDC-0051

National Snow and Ice Data Center

TABLE OF CONTENTS

1 DATA DESCRIPTION

This data set is generated from brightness temperature data derived from the following sensors: The Nimbus-7 Scanning Multichannel Microwave Radiometer (SMMR), the Defense Meteorological Satellite Program (DMSP) -F8, -F11 and -F13 Special Sensor Microwave/Imagers (SSM/Is), and the DMSP-F17 Special Sensor Microwave Imager/Sounder (SSMIS). The data are provided in the polar stereographic projection at a nominal grid cell size of 25 x 25 km.

This product is designed to provide a consistent time series of sea ice concentrations—the fraction of ocean area covered by sea ice—for the entire passive microwave record. Sea ice algorithm coefficients are calibrated to reduce differences in sea ice extent and area estimates between the SMMR, SSM/I and SSMIS sensors. The data are generated using the NASA Team algorithm developed by the Cryospheric Sciences Laboratory at the NASA Goddard Space Flight Center (GSFC).

These data include gridded daily (every other day for SMMR data) and monthly averaged sea ice concentrations for both the north and south polar regions. The data are produced at GSFC about once per year, with roughly a one-year latency. The data record begins on 26 October 1978. Data are produced from SMMR brightness temperature data processed at NASA GSFC and from SSM/I and SSMIS brightness temperature data processed at the National Snow and Ice Data Center (NSIDC).

1.1 Using these Data

Potential applications for these sea ice concentration data include:

- Monitoring the distribution, extent, and area of the Arctic and Antarctic sea ice cover
- Identifying and monitoring large, persistent open water areas surrounded by sea ice (polynyas)
- Analyses of regional and global trends in sea ice cover
- Validation of sea ice models and climate models

Analysis of sea ice/ocean and sea ice/atmosphere interactions

1.2 Parameters

1.1.1 Parameter Description

Sea ice concentration represents an areal fractional coverage of sea ice. For a given grid cell, the parameter provides an estimate of the fraction of that cell covered by sea ice, with the remainder of

the area consisting of open ocean. Grid cells consisting primarily of land are coded with a land mask value.

1.1.2 Parameter Source

Data sources include Nimbus-7 SMMR, DMSP-F8, -F11 and -F13 SSM/I instruments, and the DMSP-F17 SSMIS instrument.

1.1.3 Parameter Range

The data array stores the sea ice fraction as packed one-byte unsigned integers ranging from 0 (0%) to 250 (100%), fa sea ice concentration resolution. In addition to these valid data values, the array also holds four flag values:

- 251 indicates that the grid cell has been masked as near the "pole hole", a region near the pole where data are frequently unavailable for this satellite
- 252 indicates unused data value for a grid cell
- 253 indicates coast, i.e. land grid cell orthogonally adjacent to the ocean
- 254 indicates "land" as determined by a fixed land mask

All three flag values are generally ignored by most NetCDF software because they are outside the range of values that represent valid sea ice concentrations. Use of these flag values encodes information about the land mask and the pole hole without the need for an additional data array.

1.3 File Information

1.3.1 Format

The data are in NetCDF (.nc) format, using CF 1.6 (Climate and Forecast) and ACDD 1.3 (Attribute Conventions for Dataset Discovery) metadata conventions.

1.3.2 File Contents

The NetCDF (.nc) files come with corresponding browse image files (.png) and a granule-specific metadata file, called an Extensible Markup Language (.xml) file. CF metadata, and, when sea ice concentration is retrieved, a concentration variable (see Section 1.3.3 for further details).

1.3.3 Naming Convention

Files are named according to the following convention and as described in Table 1.

File Name Convention: `NSIDC0051_SEAICE_PS_HXXkm_YYYYMMDD_v2.0_SSS.ext`

Example Data File Name: `NSIDC0051_SEAICE_PS_N25km_20220630_v2.0.nc`

Example Browse File Name: `NSIDC0051_SEAICE_PS_N25km_20220630_v2.0_F17.png`

Table 1. File Naming Convention Description.

Variable	Description
`SEAICE`	Identifies this as a file containing sea ice concentration
`PS`	Identifies the grid as Polar Stereographic spatial reference system
`H`	Hemisphere: Northern (`N`) or Southern (`S`)
`XXkm`	Grid cell size (example: 25 km)
`YYYY`	4-digit year
`MM`	2-digit month
`DD`	2-digit day (omitted for monthly files)
`vV`	Version number (example: v2.0)
`SSS`	Sensor (`N07` for Nimbus-7 SMMR; `F08, F11, or F13` for DMSP-F8, -F11, or F13 SSM/I; `F17` for DMSP-F17 SSMIS) – only included for Browse Files
`.ext`	File extension: NetCDF (`.nc`) or PNG image file (`.png`)

On days when concentration data are available, the NetCDF file contains the concentration field in a variable of the form <SENSOR>_ICECON where the sensor may be N07, F08, F11, F13, or F17; for example, “F17_ICECON”. On days when data was not collected, the file exists but there is no <SENSOR>_ICECON variable in the file. For example, the SMMR instrument (N07) collected data only every other day, so there is a sea ice concentration field only every other day during the SMMR period (1978 to August 1987). A NetCDF file is still generated daily for SMMR, but on days without data, the N07_ICECON variable will not be present in the file. This is also the case for all other days when data is not collected, including the December 1987 to January 1988 period during the F08 SSMI operational period.

The dimensions of the <SENSOR>_ICECON variable are (t, y, x) which allows the data to be concatenated along the time dimension using standard NetCDF toolsets.

Each data file also includes a coordinate reference system variable, “crs”, in addition to associated x and y dimensions containing the center-of-grid cell locations in projected meters. This encoding allows the data to be plotted and properly georeferenced by geo-aware software such as Panoply, QGIS, GDAL tools, and others.

1.4 Spatial Information

1.4.1 Coverage

Data set coverage includes the polar regions, as defined by the Polar Stereographic Projection spatial coverage map.

Each of the three instruments provide global coverage except for a circular sector centered over the North Pole. These sectors are never measured due to orbit inclination of the satellite. Table 2 shows the sizes and latitudes of each of the pole holes.

NOTE: The SSMIS pole hole was implemented in March 2015 and applied to all data from January 2008 to present. Even though SSMIS data begin in January 2007, this product does not start using the SSMIS pole hole mask until January 2008 to allow for comparison analysis with SSM/I during the transition from SSM/I to SSMIS data in 2007.

Table 2. Pole Hole Sizes and Dates by Mask

Pole Hole Mask Name	Pole Hole Area (million km2)	Pole Hole Radius (km)	Latitude	Dates Used
SMMR Pole Hole Mask	1.19	611	84.5° N	November 1978 through June 1987
SSM/I Pole Hole Mask	0.31	311	87.2° N	July 1987 through December 2007
SSMIS Pole Hole Mask	0.029	94	89.18° N	January 2008 to present

1.4.2 Resolution

The nominal spatial resolution for this data set is 25 km. However, because the polar grids are not equal area, the actual resolution varies by latitude.

1.4.3 Projection and Grid Description

The sea ice concentration data are displayed in polar stereographic projection. The grid size varies depending on the region, as described in Table 3, Table 4, and Table 5. For more information, see Polar Stereographic Projections and Grids.

Table 3. Regional Grid Size

Region	Columns	Rows
North	304	448
South	316	332

Table 4. Geolocation Details by Projection (Hemisphere)

Projected coordinate system	**NSIDC Sea Ice Polar Stereographic North**	**NSIDC Sea Ice Polar Stereographic South**
Geographic coordinate system	Unspecified datum based upon the Hughes 1980 ellipsoid	Unspecified datum based upon the Hughes 1980 ellipsoid
Longitude of true origin	-45°	0°
Latitude of true origin	70°	-70°
Scale factor at longitude of true origin	1	1
Datum	Unspecified, based on Hughes 1980 ellipsoid	Unspecified, based on Hughes 1980 ellipsoid
Ellipsoid/spheroid	Hughes 1980	Hughes 1980
Units	meter	meter
False easting	0	0
False northing	0	0
EPSG code	3411	3412
PROJ4 string	`+proj=stere +lat_0=90 +lat_ts=70 +lon_0=-45 +k=1 +x_0=0 +y_0=0 +a=6378273 +b=6356889.449 +units=m +no_defs`	`+proj=stere +lat_0=-90 +lat_ts=-70 +lon_0=0 +k=1 +x_0=0 +y_0=0 +a=6378273 +b=6356889.449 +units=m +no_defs`
Reference	https://epsg.io/3411	https://epsg.io/3412

Table 5. Grid Details based on Hemisphere.

Hemisphere	**North Polar**	**South Polar**
Grid cell size (km)	25 × 25	25 × 25
Grid size (rows × columns)	448 × 304	332 × 316
Geolocated lower left point in grid (km)	(-3850, -5350)	(-3950, -3950)

Hemisphere	North Polar	South Polar
Nominal gridded resolution	25 km	25 km
Grid rotation	0	0
ulxmap: x-axis coord, center of upper left pixel (XLLCORNER) (km)	-3,837.5 km	-3,937.5 km
ulymap: y-axis coord, center of upper left pixel (YLLCORNER) (km)	5,837.5 km	4,337.5 km

1.5 Temporal Information

1.5.1 Coverage

Data are from 26 October 1978 through the most current processing. See the "Acquisition" section of this document for dates by instrument and platform.

1.5.2 Resolution

The SMMR instrument scanner operated only on alternate days, due to spacecraft power limitations. Therefore, SMMR data were only collected every other day. Typically, there are at least 14 days of coverage per month, although there are major data gaps in August of 1982 (04, 08, and 16 August 1982), and in August of 1984 (13 through 23 August 1984) for both polar regions.

SSM/I data were collected daily and SSMIS data continue to be collected daily. A major data gap in the SSM/I data exists from 03 December 1987 to 13 January 1988.

Sea ice concentrations are provided for each day of data and also as monthly means. The monthly means are generated by averaging all the available daily files for each individual month, excluding pixels of missing data. Refer to the Monthly Data Generation section (Section 2.4.5) of this document for more information.

2 DATA ACQUISITION AND PROCESSING

2.1 Background

The SMMR, SSM/I, and SSMIS instruments are microwave radiometers that sense emitted microwave radiation. This radiation is affected by surface and atmospheric conditions, and thus provides a range of geophysical information.

2.2 Acquisition

The combined SMMR, SSM/I, and SSMIS sea ice concentration time series is produced from brightness temperatures which can be obtained from NSIDC. The five sets of satellite data currently used to create this data stream and the time periods for which the data are available are shown in Table 6.

Known periods of time in which there are missing data for each particular sensor (SSMR and SSM/I) are listed in the Resolution section (Section 1.5.2) of this document.

Table 6. Time Periods for Data

Platform and Instrument	Time Period
Nimbus-7 SMMR	26 October 1978 through 20 August 1987
DMSP-F8 SSM/I	21 August 1987 through 18 December 1991
DMSP-F11 SSM/I	19 December 1991 through 29 September 1995
DMSP-F13 SSM/I	30 September 1995 through 31 December 2007
DMSP-F17 SSMIS	01 January 2008 through present (data acquisition is ongoing)

2.2.1 SMMR

Sea ice concentrations were processed using SMMR brightness temperatures. The SMMR brightness temperatures were processed and quality checked at GSFC (Gloersen et al. 1992). See the Nimbus-7 SMMR Polar Gridded Radiances and Sea Ice Concentrations, Version 1 data set for more details.

2.2.2 SSM/I and SSMIS

SSM/I and SSMIS brightness temperature data used to create this sea ice concentration time series are produced and distributed by NSIDC. See the DMSP SSM/I-SSMIS Daily Polar Gridded Brightness Temperatures, Version 6 data set for more details.

2.3 Derivation Techniques and Algorithms

This section is extracted from NASA Technical Memorandum 104647 (Cavalieri et al., 1997).

Sea ice concentrations for this data set were produced using a revised NASA Team algorithm that uses a different set of tie points and a different weather filter than the original NASA Team algorithm; see Descriptions of and Differences between the NASA Team and Bootstrap Algorithms

for a description of the original algorithm. The NASA Technical Memorandum 104647 (Cavalieri et al., 1997) includes information about differences, such as tie points, between the original algorithm and the revised NASA Team algorithm. In addition, the NASA Team algorithm uses different channels of the SMMR and the SSM/I-SSMIS brightness temperature data (Table 7).

Table 7. SMMR and SSM/I-SSMIS Brightness Temperature Channels

Instrument	Channels
SMMR	• Vertically and horizontally polarized (V-pol and H-pol) 18.0 GHz • V-pol 37.0 GHz
SSM/I	• V-pol and H-pol 19.3 GHz • V-pol 37.0 GHz
SSMIS	• V-pol and H-pol 19.3 GHz • V-pol 37.0 GHz

The weather filter used for the SMMR (Gloersen and Cavalieri, 1986) was found to be inadequate for the SSM/I due to the SSM/I's use of the 19.3 GHz channel (which is further up on the shoulder of the water vapor line at 22.2 GHz) rather than the 18.0 GHz channel. A different weather filter is used to reduce spurious sea ice concentrations from SSM/I that result from the presence of atmospheric water vapor, non-precipitating cloud liquid water, rain, and sea surface roughening by surface winds. This filter is a combination of the SSM/I 37.0 and 19.3 GHz channels, which effectively eliminates most of the spurious sea ice concentration measurements resulting from wind-roughening of the ocean surface, cloud liquid water, and rainfall. Another filter that is based on the 19.3 and 22.2 GHz channels is also used. The rationale behind combining the 19.3 and 22.2 GHz channels is based on the sensitivity of the 22.2 GHz to water vapor and on the need to minimize the effect of ice temperature variations at the ice edge.

2.4 Processing

2.4.1 Platform and Sensor Differences

A major obstacle to resolving these differences is the lack of sufficient overlapping data from sequential sensors. This document so far has described the basic characteristics of the SMMR, SSM/I, and SSMIS platforms and summarizes the problems encountered when deriving sea ice concentrations from brightness temperatures measured by sensors with different frequencies, different footprint sizes, different visit times, and different calibrations. The techniques employed to solve these problems, or at least reduce their impacts, include:

- Mapping the sensor data onto a common grid

- Applying a new common mask
- Addressing instrument drift
- Adjusting for land-to-ocean spillover
- Replacement/omission of bad data
- Inter-sensor corrections made to reduce remaining measurement differences

Basic limitations also arise from the sensor resolution, temporal coverage, and algorithm assumptions and characteristics. The NASA Team algorithm is not designed to provide ice concentration for freshwater ice, e.g., lake and river ice. The filtering used to remove land-to-ocean spillover may affect the area of some open water features within the ice pack near coasts such as coastal polynyas.

Comparisons of sea ice concentrations calculated for each sensor during overlap periods using published algorithm tie points reveal significant differences. These may result from differences in sensor and orbital characteristics, differences in observation times (and therefore tidal effects), and/or differences in algorithm coefficients. Sensor and orbital characteristic differences for the Nimbus-7 SMMR and DMSP-F8 SSM/I include antenna beam width, channel frequency, spacecraft altitude, ascending node time, and angle of incidence. In addition, the sea ice algorithm tie points are significantly different. The DMSP sensors also differ in ascending node time, altitude, and angle of incidence. Because the visit times of the DMSP satellites occur during different phases of the diurnal cycle, tidal effects may result in differences in the sea ice distribution. It is presumed that any such effects are mitigated by the correction scheme described below. The GSFC processing attempts to accommodate for these differences in each pair of sensors by employing a set of algorithm tie points determined through linear relationships between the observed brightness temperatures during the overlap periods.

2.4.1.1 Nimbus-7 SMMR to DMSP-F8 SSM/I Transition

Daily brightness temperature maps from the Nimbus-7 SMMR and from the DMSP-F8 SSM/I during their period of overlap, 09 July to 20 August 1987, were compared for both the Arctic and Antarctic. Unfortunately, there were only 22 days of common coverage. A linear, least-squares best-fit of the cumulative data was obtained for each of the corresponding channels. For the purpose of eliminating spurious brightness temperatures resulting from residual land spillover effects, an Arctic land mask that expanded three to four pixels out from the original land mask was used in the determination of the best fit between the two data streams.

The eliminated pixels represent only a very small fraction of the total number of sea ice concentration pixels, but eliminating them helps considerably in reducing the outliers on the scatter plots. These linear relations were used to generate a set of SSM/I tie points that are consistent with the original SMMR sea ice algorithm tie points (Gloersen et al., 1992). The published DMSP-F8 SSM/I tie points (Cavalieri et al., 1992) were not used. In addition to using these transformations,

the DMSP-F8 SSM/I open water tie points were subjectively tuned to help minimize the differences between the SMMR and DMSP-F8 SSM/I sea ice extent and area during the overlap period. In all cases, except for the Antarctic DMSP-F8 SSM/I values, the tuned amount is within one standard error of estimate. GSFC suspects the reason for the larger tuned values results from greater weather effects during the overlap period.

For more information on the regression coefficients and revised tie points, see the NASA Technical Memorandum 104647 (Cavalieri et al., 1997).

2.4.1.2 DMSP-F8 to DMSP-F11 SSM/I Transition

The transition period from DMSP-F8 to -F11 includes only 16 days of good data overlap, from 03 to 18 December 1991. The DMSP-F11 SSM/I open water tie points were also tuned to help reduce differences in sea ice extent and area as was done with the DMSP-F8 SSM/I values. A further adjustment to the Antarctic 37V sea ice type-B F11 tie point was also made to reduce the sea ice area difference. In this case, the amount of tuning needed to reduce the sea ice extent and area differences between the DMSP-F8 and -F11 values is well within one standard error of estimate.

2.4.1.3 DMSP-F11 to DMSP-F13 SSM/I Transition

The effects of changing from the DMSP-F11 to the -F13 satellite were examined for a 5-month overlap period, from 5 May 1995 through 30 September 1995. Generally, in terms of hemispheric averages of mean ice concentration, the biases introduced by the transition are slight and not statistically significant; however, in some regions relatively large and significant differences are seen. In addition, differences in sea ice extent and total ice-covered area between the two platforms were found to be statistically significant. For more information, please see *the NSIDC Special Report 5: An Intercomparison of DMSP F11- and F13-derived Sea Ice Products* (Stroeve, Li, & Maslanik, 1997).

2.4.1.4 DMSP-F13 SSM/I to DMSP-F17 SSMIS Transition

The effects of changing from the DMSP-F13 SSM/I to the -F17 SSMIS were examined for a 12-month overlap period, from 01 January 2007 to 31 December 2007. Differences in sea ice extent and total ice-covered area between the two platforms and instruments were found to be statistically significant, though fairly similar when compared with previous intersensor calibrations conducted for this time series (Cavalieri et al., 1999). Earlier intersensor calibrations, however, were limited by relatively short periods of sensor overlap (such as sixteen days) and could thus account for less agreement with this transition (Cavalieri et al., 2012). In addition, earlier agreement may be due to the subjective tuning of some tie-points that was required in past intercalibrations (Cavalieri et al., 1999).

2.4.2 Land-to-Ocean Spillover and Residual Weather-Related Effects

The next step in preparing the data is the correction for land-to-ocean spillover, often referred to as "land contamination," and residual weather-related effects. While these steps eliminate much of the land-to-ocean spillover and weather effects over open ocean, these problems are not entirely removed. See the Data Verification by Data Center section (Section 2.5.3) for additional comments.

2.4.2.1 Land-to-Ocean Spillover

Land-to-ocean spillover refers to the issue of the blurring of sharp contrasts in brightness temperature, such as those that exist between land and ocean, due to the relatively coarse width of the sensor antenna pattern. This problem is of concern because it results in false sea ice signals along coastlines because both land and sea ice have much higher brightness temperatures than ocean. The method used to reduce the spillover is an extension of the method employed for the single-channel Nimbus-5 Electrically Scanning Microwave Radiometer (ESMR) data in Parkinson et al. (1987). Figure 1a illustrates the effect of the coarse resolution of the microwave antenna on a coastline resulting in false sea ice signals in the vicinity of the coast, and Figure 1b shows the seven-by-seven array used in the procedure to reduce the land-to-ocean spillover effect. The rationale behind the approach is that a minimum observed sea ice concentration in the vicinity of coastlines where no sea ice remains offshore, which is generally seen in late summer, is probably the result of land spillover; so, it is subtracted from the image. To reduce the error of subtracting sea ice in areas of actual sea ice cover, the technique searches for and requires the presence of open water in the vicinity of the image pixel to be corrected.

Land-to-ocean spillover was reduced by the following three-step procedure:

1. A matrix M was created covering the entire grid and identifying each pixel as land, shore, near-shore, offshore, or non-coastal ocean. The identification of land pixels was straightforward; they were obtained from the land/sea mask (see NASA Technical Memorandum 104625 [Martino et al., 1995]). The identification of shore, near-shore, and offshore pixels was based on the scheme shown in Figure 1b, where the pixel to be identified is labeled I,J. This pixel can be considered a *shore* pixel if any pixel adjacent to it is land, a *near-shore* pixel if none of the A pixels are land but at least one of the B pixels is land, and an *offshore* pixel if none of the A or B pixels are land but at least one of the C pixels is land. All other ocean pixels are considered *non-coastal ocean*. This matrix M is created once and used throughout the data set.

2. A matrix CMIN, to represent minimum sea ice concentrations on a pixel-by-pixel basis throughout the entire grid, was created for each instrument type. CMIN was created by first constructing a matrix P containing the minimum monthly average sea ice concentrations throughout a given year, then adjusting that matrix at *offshore*, *near-shore*, and *shore* pixels. In the case of SMMR, 1984 monthly data were used, whereas in the case of SSM/I, 1992 monthly data were used. In both cases, the adjustments were as follows: (a) at offshore pixels, any P values exceeding 20% were reduced to 20 percent; (b) at near-shore

pixels, any P values exceeding 40% were reduced to 40 percent; and (c) at shore pixels, any P values exceeding 60% were reduced to 60 percent. The CMIN matrix was created once for SMMR and once for SSM/I, then used throughout the data set.

3. The daily sea ice concentration matrices were adjusted at any *offshore*, *near-shore*, and *shore* pixels in the vicinity of open water. Specifically, the **neighborhood** of an *offshore* pixel was defined as containing the 8 other pixels in the 3 x 3 box centered on the *offshore* pixel; the **neighborhood** of a *near-shore* pixel was defined as containing the 24 other pixels in the 5 x 5 box centered on the *near-shore* pixel; and the **neighborhood** of a *shore* pixel was defined as containing the 48 other pixels in the 7 x 7 box centered on the *shore* pixel. At any time when the neighborhood of an *offshore*, *near-shore*, or *shore* pixel contains three or more open-water pixels (sea ice concentration less than 15 percent), then the calculated sea ice concentration at the *offshore*, *near-shore*, or *shore* pixel is reduced by the value for that pixel in the matrix CMIN. Wherever the subtraction leads to negative sea ice concentrations, the concentrations are set to 0 percent. This land-spillover correction algorithm is clearly a rough approximation, as the contaminated amount does not stay constant over time; but the scheme has been found to reduce substantially the spurious sea ice concentrations on the grids.

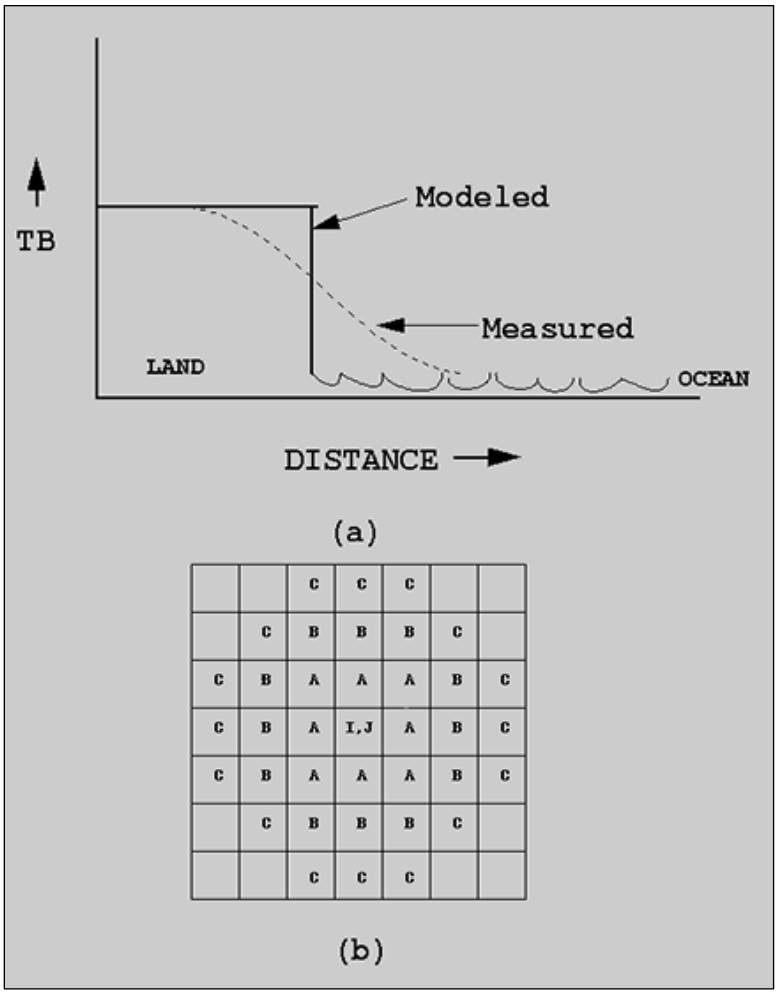

Figure 1. (a) Effect of the coarse resolution of the microwave antenna on a coastline resulting in false sea ice signals in the vicinity of the coast. (b) Seven-by-seven array used in the procedure to reduce the land-to-ocean spillover effect.

2.4.2.2 Residual Weather-Related Effects

Weather effects can cause the passive microwave signature of seawater to appear like that of ice (Cavalieri, St. Germain, and Swift, 1995). A correction is made for removing spurious ice resulting from residual weather effects that were missed by the automatic weather filters. These valid ice masks are based on monthly climatological Sea Surface Temperatures (SSTs) from the NOAA Ocean Atlas (Levitus and Boyer, 1994). These data, originally on a two-degree by two-degree grid, were remapped onto the SSM/I grid. Because the SST data did not extend to the SSM/I coastline, the data were extrapolated to the coastline once they were mapped onto the SSM/I grid. The SST maps are used as follows:

- In the Northern Hemisphere, in any pixel where the monthly SST is greater than 278 K, the sea ice concentration is set to zero throughout the month.

- In the Southern Hemisphere, in any pixel where the monthly SST is greater than 275 K, the sea ice concentration is set to zero throughout the month.
- The higher threshold SST value was needed in the Northern Hemisphere because the 275 K isotherm used in the south was too close to the sea ice edge in the north. In a few instances, corrections to the regridded SST data were needed, because otherwise actual sea ice was being lost.

2.4.3 Manual Quality Control

The automated residual weather removal procedures unfortunately do not remove all spurious ice. Particularly in the older data, clearly erroneous sea ice concentration values occurred on occasion due to bad input brightness temperatures, sometimes even with entire scans or swaths being dominated by bad data. Consequently, a manual quality control procedure was used to remove these erroneous data. This is done by visual inspection of the ice concentration images. In some instances, the erroneous nature of the data is quite clear, while in other instances it is less definitive. In the latter cases, a decision to retain or remove the suspect data is made based on consistency or lack of consistency with the data for the preceding and succeeding days. For data deemed to be spurious in the open ocean region, the ice concentrations are zeroed out. Data deemed to be erroneous within the ice cover are flagged as missing data and are filled like other data gaps, as described below.

2.4.4 Filling Data Gaps

There are instances of missing data. In some cases, whole days (or weeks or months) are missing. In other cases, large swaths or wedges of missing data exist within an image, along with scattered pixels of missing data throughout the grid. The scattered pixels of missing data, resulting generally from mapping the orbital data to the SSM/I grid, were filled by applying a spatial linear interpolation scheme on the brightness temperature maps. The larger areas of missing data, resulting from gaps between orbital swaths (generally at low latitudes on daily maps) or from partial coverage or missing days, were filled by temporal interpolation on the sea ice concentration maps. No data whatsoever were available for the period from 02 December 1987 through 12 January 1988. This gap was not filled by temporal linear interpolation; instead, it was left as missing data.

2.4.5 Monthly Data Generation

Once the daily data have been processed as previously described, monthly data are generated. Monthly averaged sea ice concentration grids are produced from an average of the daily sea ice concentration grids available for each month. Monthly files for both hemispheres are provided for every month beginning October 1978. However, for October 1978, December 1987 and January 1988, the time series was incomplete: only three days of data were available during October 1978 to generate the monthly mean, only two days were available for December 1987, and only 19 days

were available for January 1988. Therefore, the monthly means for these months are not “true” representations of the monthly means.

In most cases, GSFC used all daily data to compute monthly averaged sea ice concentrations from a particular instrument until the data were no longer available. For example, SMMR data were used to compute monthly sea ice concentrations until the instrument stopped collecting data on 20 August 1987. Beginning 21 August 1987, SSM/I data were used. In 1991, DMSP-F8 SSM/I data were used through December 18; beginning December 19, DMSP-F11 SSM/I data were used.

Note: It is recommended that sea ice extent and area be computed from daily maps of ice concentrations that are then used to compute monthly averages of those parameters. Computations of sea ice extents and sea ice areas should not be made from the monthly-averaged ice concentration maps because that may result in a biased time series.

2.5 Quality, Errors, and Limitations

Users should be aware that the ice concentration maps were derived from algorithms that were calibrated to minimize the differences in ice extent and ice-covered area during the overlap periods when transitioning from one instrument to the next (overlap from SMMR to DMSP-F8 SSM/I, from DMSP-F8 to -F11 SSM/I, from DMSP-F11 to -F13 SSM/I, and from DMSP-F13 SSM/I to DMSP-F17 SSMIS). This does not mean that the ice concentrations themselves are well matched. See the Data Verification by Data Center section (Section 2.5.3) of this document for a summary of ice extent and ice-covered area differences during the overlap periods.

It is also important to note that SMMR and SSM/I-SSMIS have different data gaps at the North Pole due to orbital differences. Therefore, any time series of parameters, such as ice extent and ice-covered area, need to take these differences into account. A pole mask is provided for this purpose. See the polar stereographic tools help article for details on masks and overlays.

Particular care is needed to interpret the sea ice concentrations during summer when melt is present, and in regions where new sea ice makes up a substantial part of the sea ice cover. Some residual errors remain due to weather effects and mixing of ocean and land area within the sensor field of view (FOV), and due to sensor differences.

It is recommended sea ice extent and area be computed from daily grids of ice concentrations that are then used to compute monthly averages of those parameters. Computations of sea ice extents and sea ice areas should not be made from the monthly-averaged ice concentration maps because that may result in a biased time series.

2.5.1 Data Validation by Source

The performance of the NASA Team algorithm has been assessed by the data providers in several studies, including: Cavalieri et al., 1991; Cavalieri et al., 1992; Cavalieri et al., 1999. In early years, the data providers made improvements to their processing, including reducing errors due to coastal and weather influences. The most recent significant changes in the processing were made in 1999, and processing methodology has remained consistent since then except for adjustments made for sensor transitions. Table 8 and Table 9 summarize the comparison between the ice-covered areas and ice extent during the overlap periods, including mean differences and linear regression results of ice-covered areas and ice extent. Mean differences are computed for SMMR minus DMSP-F8 SSM/I, DMSP-F8 SSM/I minus DMSP-F11 SSM/I, DMSP-F11 SSM/I minus DMSP-F13 SSM/I, and DMSP-F13 SSM/I minus DMSP-F17 SSMIS. Regression coefficients are computed using y = a0 + a1*x, for each (x, y) pair (x = SMMR, y = DMSP-F8 SSM/I); (x = DMSP-F8 SSM/I, y = DMSP-F11 SSM/I); (x = DMSP-F11 SSM/I, y = DMSP-F13 SSM/I); and (x = DMSP-F13 SSM/I, y = DMSP-F17 SSMIS). While this analysis shows no significant differences between the overall summaries of ice-covered area and ice extent, significant regional differences in ice concentration may still be present.

Table 8. Northern Hemisphere Sensor Differences

	Mean Difference (x $10^6 km^2$)	Standard Deviation (x $10^6 km^2$)	a_0 (x 10^6)	a_1 (x 10^6)	Correlation Coefficient	% Difference
SMMR to DMSP-F8 SSM/I						
Ice area	0.073	0.054	0.214	0.947	0.999	1.34%
Ice extent	0.055	0.096	0.412	0.941	0.998	0.70%
DMSP-F8 to DMSP-F11 SSM/I						
Ice area	-0.019	0.036	0.955	0.914	0.996	0.18%
Ice extent	0.002	0.058	0.351	0.972	0.983	0.01%
DMSP-F11 to DMSP-F13 SSM/I						
Ice area	-0.0112	0.0296	0.0079	0.997	0.999	0.18%
Ice extent	-0.0004	0.0457	0.0199	0.997	0.999	-0.01%
DMSP-F13 to DMSP-F17 SSMIS						
Ice area	-0.0389	0.0188	0.0329	1.0007	0.999	0.5433%
Ice extent	-0.0027	0.0426	-0.0297	1.0032	0.999	-0.0156%

Table 9. Southern Hemisphere Sensor Differences

	Mean Difference (x $10^6 km^2$)	Standard Deviation (x $10^6 km^2$)	a_0 (x 10^6)	a_1 (x 10^6)	Correlation Coefficient	% Difference
SMMR to DMSP-F8 SSM/I						
Ice area	0.018	0.072	0.225	0.982	0.992	0.15%
Ice extent	0.005	0.058	-0.198	1.011	0.998	0.0%
DMSP-F8 to DMSP-F11 SSM/I						
Ice area	-0.038	0.092	0.630	0.924	0.996	0.49%
Ice extent	0.012	0.067	0.289	0.974	0.998	0.08%
DMSP-F11 to DMSP-F13 SSM/I						
Ice area	0.0311	0.0344	-0.0474	1.007	0.999	0.26%
Ice extent	0.0126	0.0402	-0.0186	1.002	0.999	0.08%
DMSP-F13 to DMSP-F17 SSMIS						
Ice area	-0.0212	0.0314	-0.0097	1.0034	0.999	0.1550%
Ice extent	-0.0009	0.0309	0.0109	0.9992	0.999	0.0304%

2.5.2 Confidence Level/Accuracy Judgment

Estimates of the accuracy of the NASA Team algorithm vary depending on sea ice conditions, methods, and locations used in individual studies. Cavalieri et al. (1992) summarizes several of these studies. In general, accuracy of total sea ice concentration is within +/- 5 percent of the actual sea ice concentration in winter, and +/- 15 percent in the Arctic during summer when melt ponds are present on the sea ice. However, accuracy at a specific location and time can vary widely. Accuracy tends to be best within the consolidated ice pack when the sea ice is relatively thick (greater than 20 cm) and ice concentration is high. Accuracy decreases as the proportion of thin ice increases. See Cavalieri et al. (1991), Ivanova et al. (2014), Kern et al. (2019), Kern et al. (2020), Maslanik (1992), Meier (2005), and Steffen & Schweiger (1991) for an overview of the algorithm performance.

2.5.3 Data Verification by Data Center

NSIDC staff visually check the data files and selected graphics files. This includes verification of proper file structure; comparisons to existing SMMR-, SSM/I-, and SSMIS-derived sea ice concentration grids, masks, and information files; and examination of data quality.

Some weather-related effects and land contamination often remain even after the automated and manual corrections are applied. The amount and spatial distribution of remaining weather effects vary with season. Also, occasional bad scan lines still appear in the data. Based on NSIDC analyses, some sensor-to-sensor differences are likely to remain in these data, particularly for marginal ice zones. See *NSIDC Special Report 5: An Intercomparison of DMSP F11- and F13-derived Sea Ice Products* (Stroeve et al., 1997) for summaries of differences among the SSM/I sensors.

Residual weather effects and processing errors in May 1986 data result in large bands of very low ice concentrations over the open ocean in the Weddell, Bellingshausen, and Amundsen Seas in the Southern Hemisphere. Although the magnitude of these false ice concentrations is less than one percent, users should be aware that such errors do occur in data for many days within that month.

While this data set only provides data from one instrument on a given day, overlap periods exist when data are available from more than one instrument. Analysis of these overlap periods allowed researchers to calibrate the sea ice algorithms so that the ice concentration fields are consistent across sensor transitions. Details of the instrument intercalibration are provided in Cavalieri et al. (1999) and Cavalieri et al. (2012).

2.6 Instrumentation

2.6.1 Description

The SMMR, SSM/I, and SSMIS Sensors Summary describes each instrument.

3 SOFTWARE AND TOOLS

The data are provided in NetCDF format and can be read and viewed using software capable of interpreting this standard format. NASA's Panoply (https://www.giss.nasa.gov/tools/panoply/) visualization software and the NetCDF Operator NCO (http://nco.sourceforge.net/) suite of command line tools have been used extensively at NSIDC to work with these data. A script housed on Github (https://github.com/nsidc/polarstereo-reformat) converts the NetCDF back to the original binary format.

For a list of all polar stereographic tools and for more information, see the Polar Stereographic Data web page.

4 VERSION HISTORY

Table 10 summarizes the Version history for this product.

Table 10. Version History Table

Version	Date	Description
V2	Sept 2022	Version reflects conversion of the data set format from binary to NetCDF.
V1.1	Dec 2015	Data were reprocessed from 1978 to 2014, and additional QC of the data set was done to remove additional spurious ice. In addition, the data set no longer includes overlap dates during satellite transition periods. This version also extends the temporal coverage through the present.
V1	Mar 2015	SSMIS pole hole mask replaces SSM/I pole hole mask for all data from 01 January 2008 to present.
V1	Jul 2014	An error was found in the sea ice concentration field for 14 September 1984. Due to a geolocation error in the source data, several hundred thousand square kilometers of erroneous ice occurred in that data. The original file has been removed and replaced with an average of the two files nearest in time (September 12 and 16). The monthly September 1984 average concentration field was reprocessed using the replaced September 14 data.
V1	Jun 2014	The browse images for the entire record have been reprocessed to include a title and simplified color bar; the data were not affected.
V1	Jan 2013	NSIDC applied corrections to 29 files that showed errors in a previous release of these data. The errors occurred in files from both SMMR (1983 – 1985) and SSM/I (1995 – 1996).
V1	Jan 1996	Original version of data.

5 RELATED DATA SETS

Near-Real-Time DMSP SSM/I-SSMIS Daily Polar Gridded Sea Ice Concentrations

Bootstrap Sea Ice Concentrations from Nimbus-7 SMMR and DMSP SSM/I

Sea Ice Index

Sea Ice Trends and Climatologies from SMMR and SSM/I-SSMIS

Sea Ice Remote Sensing at NASA Goddard Space Flight Center

Polar Stereographic Ancillary Grid Information

6 ACKNOWLEDGMENTS

The authors are grateful to Walter N. Meier, James S. Stewart, Hannah Wilcox, Donna J. Scott, Molly A. Hardman, and Jessica Calme.

7 REFERENCES

Cavalieri, D. J., J. Crawford, M. Drinkwater, W. J. Emery, D. T. Eppler, L. D. Farmer, M. Goodberlet, R. Jentz, A. Milman, C. Morris, R. Onstott, A. Schweiger, R. Shuchman, K. Steffen, C. T. Swift, C. Wackerman, and R. L. Weaver. 1992. *NASA Sea Ice Validation Program for the DMSP SSM/I: Final Report.* NASA Technical Memorandum 104559. National Aeronautics and Space Administration, Washington, D. C. 126 pages, https://ntrs.nasa.gov/citations/19920015007.

Cavalieri, D. J., J. Crawford, M. R. Drinkwater, D. Eppler, L. D. Farmer, R. R. Jentz and C. C. Wackerman. 1991. Aircraft Active and Passive Microwave Validation of Sea Ice Concentration from the DMSP SSM/I. *Journal of Geophysical Research* 96(C12):21,989-22,009, https://doi.org/10.1029/91JC02335.

Cavalieri, D. J., K. M. St. Germain, and C. T. Swift. 1995. Reduction of Weather Effects in the Calculation of Sea Ice Concentration with the DMSP SSM/I. *Journal of Glaciology*. 41(139):455-464, https://doi.org/10.3189/S0022143000034791.

Cavalieri, D.J., C.L. Parkinson, N. DiGirolamo, A. Ivanoff. 2012. Intersensor Calibration Between F13 SSMI and F17 SSMIS for Global Sea Ice Data Records. *IEEE Geoscience and Remote Sensing Letters*, 9(2), 233-236, https://doi.org/10.1109/LGRS.2011.2166754.

Cavalieri, D. J., C. L. Parkinson, P. Gloersen, J. C. Comiso, and H. J. Zwally. 1999. Deriving Long-term Time Series of Sea Ice Cover from Satellite Passive-Microwave Multisensor Data Sets. *Journal of Geophysical Research* 104(7): 15,803-15,814, https://doi.org/10.1029/1999JC900081.

Cavalieri, D. J., C. L. Parkinson, P. Gloersen, and H. J. Zwally. 1997. *Arctic and Antarctic Sea Ice Concentrations from Multichannel Passive-microwave Satellite Data Sets: October 1978 to*

September 1995, User's Guide. NASA Technical Memorandum 104647. 17 pages. (PDF)

Gloersen P. and D. J. Cavalieri. 1986. Reduction of Weather Effects in the Calculation of Sea Ice Concentration from Microwave Radiances. *Journal of Geophysical Research* 91(C3):3913-3919, https://doi.org/10.1029/JC091iC03p03913.

Gloersen P., W. J. Campbell, D. J. Cavalieri, J. C. Comiso, C. L. Parkinson, H. J. Zwally. 1992. *Arctic and Antarctic Sea Ice, 1978-1987: Satellite Passive Microwave Observations and Analysis.* NASA Special Publication 511, https://ntrs.nasa.gov/citations/19940012966.

Ivanova, N., O. M. Johannessen, L. T. Pedersen, and R. T. Tonboe. 2014. Retrieval of Arctic sea ice parameters by satellite passive microwave sensors: A comparison of eleven sea ice concentration algorithms, *IEEE Trans. Geosci. Rem. Sens*., 52(11), 7233-7246, https://doi.org/10.1109/TGRS.2014.2310136.

Kern, S., T. Lavergne, D. Notz, L. T. Pedersen, R. T. Tonboe, R. Saldo, and A. M. Sørensen. 2019. Satellite passive microwave sea-ice concentration data set intercomparison: closed ice and ship-based observations, *The Cryosphere*, 13, 3261–3307, https://doi.org/10.5194/tc-13-3261-2019.

Kern, S., T. Lavergne, D. Notz, L. T. Pedersen, and R. Tonboe. 2020. Satellite passive microwave sea-ice concentration data set inter-comparison for Arctic summer conditions, *The Cryosphere*, 14, 2469–2493, https://doi.org/10.5194/tc-14-2469-2020.

Levitus, S. and Boyer, T. P. 1994. World Ocean Atlas 1994, Volume 4: Temperature, NOAA National Oceanographic Data Center, Ocean Climate Laboratory, U.S. Department of Commerce, Washington D.C., https://repository.library.noaa.gov/view/noaa/1381.

Martino, M. G., D. J. Cavalieri, P. Gloersen, and H. J. Zwally. 1995. *An Improved Land Mask for the SSM/I Grid*. Edited by J. G. Acker. NASA Technical Memorandum 104625. 9 pages. (PDF)

Maslanik, J. A. 1992. Effects of Weather on the Retrieval of Sea Ice Concentration and Ice Type from Passive Microwave Data. *International Journal of Remote Sensing*, 13(1):37-54, https://doi.org/10.1080/01431169208904024.

Meier, W. N. 2005. Comparison of passive microwave ice concentration algorithm retrievals with AVHRR imagery in the Arctic peripheral seas, IEEE *Trans. Geosci. Rem. Sens*., 43(6), 1324-1337, https://doi.org/10.1109/TGRS.2005.846151.

Parkinson, C. l., J. C. Comiso, H. J. Zwally, D. J. Cavalieri, P. Gloersen, and W. J. Campbell. 1987. *Arctic Sea Ice, 1973-1976: Satellite Passive-Microwave Observations,* NASA SP-489,

National Aeronautics and Space Administration, Washington, D. C. 296 pages, https://apps.dtic.mil/sti/citations/ADA278193.

Steffen, K. and A. Schweiger. 1991. NASA Team Algorithm for Sea Ice Concentration Retrieval from Defense Meteorological Satellite Program Special Sensor Microwave/Imager: Comparison with Landsat satellite imagery. *Journal of Geophysical Research*, 96(C12):21971-21987, https://doi.org/10.1029/91JC02334.

Stroeve, J., X. Li, and J. Maslanik. 1997. NSIDC Special Report 5: An Intercomparison of DMSP F11- and F13-derived Sea Ice Products. Boulder, CO: National Snow and Ice Data Center. (PDF)

8 DOCUMENT INFORMATION

8.1 Publication Date

September 2023

8.2 Date Last Updated

September 2023